Energy Reports 13 (2025) 4087–4094

Contents lists available at ScienceDirect

Energy Reports

journal homepage: www.elsevier.com/locate/egyr

Research paper

Heliostat accurate control method robust under shading and blocking

Irjuwan Abunajeeb [a], Gideon Stein [a,b], Carmel Rotschild [a,b,*]

[a] Technion, Israel Institute of Technology, Grand Technion Energy Program GTEP, Israel
[b] Technion, Israel Institute of Technology, Mechanical Engineering Department, Israel

ARTICLE INFO

Keywords:
Concentrated solar power
Optical efficiency
Heliostat control

ABSTRACT

Concentrated Solar Power [CSP] technologies address one of the challenges associated with intermittent energy sources such as wind and solar by incorporating thermal energy storage [TES], allowing generation to be shifted to periods without solar resources, and providing backup energy during periods with reduced sunlight that can be caused by cloud cover. Furthermore, CSP's ability to operate on gas when TES runs out offers a base load and dispatchable renewable solution in the systems that use a gas generator as a backup, which in the future can rely on hydrogen. Enhancing optical efficiency is a key challenge in CSP technology development, which requires wirelessly controlling the exact aiming orientation of tens of thousands of heliostats within sub-milliradian accuracy, while optically monitoring the field from outside the optical path where a very high temperature is obtained. Another challenge is the minimal number of pixels designated to each heliostat, as the entire solar field is monitored simultaneously. Optical efficiency optimization is also challenging due to the inherent tradeoff between the Ground Cover Ratio (GCR) and the shading and blocking of the mirrors. The heliostat control method proposed in this paper is applicable to solar power tower technology. This study aims to improve the accuracy of the solar field's tracking under shading and blocking by presenting and implementing a novel tracking method and comparing it to prior art. The method is based on monitoring the reflection from a specular curved bar along the vertical and the horizontal edge of the heliostat (or mirror facet). According to the place of the sun's reflection, the deviation from the receiver is obtained. The results show that the triangulation method using a specular curved bar gives an accuracy of 0.8 mrad, which is superior to the prior art, considering shading and blocking. It also provides the best accuracy in the exploitation of pixels. This enhancement in efficiency will bring us closer to achieving 90–95 % availability of renewable electricity at the cost of gas. This advancement stands as a significant stride in our ongoing battle against climate change.

1. Introduction

CSP is an essential technology in the field of renewable energy, which can offer both baseload and dispatchable power. This is true in the systems that use a gas generator as a backup, which in future can rely on hydrogen. CSP towers with storage systems can store energy for up to 10–15 h, depending on the specific system's capacity and design. The percentage of time a gas generator would be needed can vary depending on the location and the solar resource availability, but typically, gas backup might be used for around 5–10 % of the time, especially in areas where solar radiation is highly variable. In regions with consistent sun, the need for backup is significantly reduced, and some systems are designed to operate with minimal or no fossil fuel use. It has several advantages, and its contribution to the global effort to transition to more sustainable and environmentally friendly energy sources is estimated to increase. This is because CSP technologies address one of the challenges associated with intermittent energy sources such as wind and solar by incorporating TES, allowing generation to be shifted to periods without solar resources, and providing backup energy during periods with reduced sunlight that can be caused by cloud cover (Sioshansi and Denholm, 2010; Palacios et al., 2020). So, CSP with thermal storage is a more dispatchable and flexible technology compared to wind and PV without storage, making it capable of providing spinning reserves and other ancillary services. This ability to respond to sudden shifts in demand or supply enhances grid stability, making CSP an important tool in integrating renewables into the energy mix. In addition, electric power generation can run on gas when storage ends, offering a baseload solution that emerges as a cost-competitive option among other sources of renewable energy (Palacios et al., 2020; del Ríoa et al., 2018).

Many researchers focus on improving CSP technology by enhancing

* Corresponding author at: Technion, Israel Institute of Technology, Grand Technion Energy Program GTEP, Israel.
E-mail address: carmelr@technion.ac.il (C. Rotschild).

https://doi.org/10.1016/j.egyr.2025.03.047
Received 2 January 2025; Received in revised form 11 March 2025; Accepted 26 March 2025
Available online 2 April 2025

thermal energy storage (Sioshansi and Denholm, 2010; Palacios et al., 2020), heat transfer fluids efficiency (Reddy and Khan, 2022), power-generating devices and techniques (Md Tasbirul et al., 2018), and optical efficiency (Hu et al., 2021; Sánchez-González et al., 2020). Other studies have focused on the design of the heliostat field system, causing the sun's incident angle on the heliostat to get smaller, thus increasing the effective area of the solar field (Hu et al., 2021). Future research in CSP should also focus on mirror facet cleaning strategies and heliostat operation and maintenance (O&M) to enhance long-term performance, reduce soiling losses, and improve overall system efficiency. Optical efficiency deals with the problem of not all the solar radiation reaching the heliostats being concentrated on the target. Specifically, we are concerned with direct solar radiation and not diffused radiation.

Enhancing optical efficiency is a main challenge in CSP technology development. Optical errors are categorized in many categories: sun-shape errors and brightness distributions that are caused by the shape of the reflectors and the atmospheric conditions, specularity errors that are related to the collector's mirror quality, surface slope errors that are caused by imperfections in the mirror surface, misalignment errors of the facets (Sánchez-González et al., 2020; Coquand et al., 2017) and the tracking error or the angular offset from the target (El Ydrissi et al., 2019). The tracking errors may be caused by many sources, including angular offset in the reference position of the tracking mechanisms, imperfect leveling of the heliostat pedestal, lack of perpendicularity between the tracking axes, and lack of precise clock synchronization (Christoph Sattler et al., 2020). Solar field efficiency is also affected by shading and blocking of the heliostats according to the specific field distribution (Christoph Sattler et al., 2020; Rizvi and Yang, 2022), which conventionally aims to increase GCR. Precise solar tracking is essential for the efficiency of CSP systems (He et al., 2013; Díaz-Félix et al., 2014). Heliostats accurately track the sun's movement throughout the day to reflect sunlight onto a central receiver or tower. This tracking ensures that the concentrated sunlight remains focused on the receiver for maximum energy capture. Moreover, a highly accurate tracking system can lead to a reduction in spillage losses as well as a better flux distribution on the receiver. This, in turn, can increase efficiency and thus have a positive effect on the levelized cost of electricity (LCOE) (Christoph Sattler et al., 2020).

The heliostat control system can be divided into two parts: 1. rough heliostat orientation using, for example, an accelerometer to move the mirror to a parking orientation (Google, 2025), keep flux off-target, or get the reflected light spot close enough to the receiver target to ease the application of precise tracking techniques, and 2. precise on-target control. Advances in materials, sensors, and control algorithms have contributed to the continued improvement of heliostat on-target tracking systems in CSP applications.

Research focused on continuous alignment of the heliostat includes two main types of heliostat on-target tracking: open-loop and closed-loop. Errors due to open-loop tracking control are often around 1–2 mrad and can accumulate during operation (Kribus et al., 2004). The solution should be a closed-loop control method that can work dynamically, detecting errors and sending feedback signals to the algorithm without interfering with the receiver operation. Heliostat closed-loop control methods are classified into four categories according to the location of the primary device required for the calibration method, type, and number of measuring devices or sensors (Christoph Sattler et al., 2020). The first class is based on central cameras or sensors. The cameras or sensors may be on the ground (Krupkin and Yogev, 1999) or on the tower (Hines and Johnson, 2012; Zavodny et al., 2015). The estimated accuracies of such methods may be in the range of 0.1–10 mrad, but the problem with this method is that it is too slow for closed-loop control. The second class is central laser or radar-based measurement methods (Klimek et al., 2012) with an estimated measurement accuracy of 0.43–1.1 mrad. However, the control needs a few minutes to be implemented, which is not preferred for closed-loop control. The third class is cameras or sensors on each heliostat (Bern et al., 2017): the estimated measurement accuracy is 0.13–1 mrad. The fourth class is central solar focus position detection with cameras or sensors on the tower: the estimated measurement accuracy is 0.1–0.3 mrad (Christoph Sattler et al., 2020), such as a tracking method announced by Yogev and Krupkin (1999) and was first implemented by Kribus et al. (2004). This method requires the installation of four cameras around the receiver and directed towards the solar field to measure how much deviation each heliostat has from the aiming point by comparing the captured power differences from that heliostat. However, this method is challenged when shading and blocking are significant. A demonstration at Sandia National Laboratories' National Solar Thermal Test Facility (NSTTF), Heliogen showcased their ability to reduce heliostat tracking errors to 0.33 milliradians (mrad). This was achieved through their advanced control software, which integrates computer vision and real-time adjustments to optimize the heliostat positioning (Anon, 2023). Our experiment report is that sub-millirad accuracy is achievable using our method. **It is the aim of this paper to present an accurate tracking method based on triangulation that is robust under shading and blocking,** and experimentally compare our results with the Kribus method (Kribus et al., 2004). Our method is offering a closed loop control. Closed loop control is continuously correcting the heliostat direction against all the factors in addition to the sun movement, including wind drifts and soil movements.

2. Methodology

2.1. Triangulation method (curved bars having a circular arc)

The method is based on placing curved bars having a circular arc along the edges of the heliostat (or mirror facet) (see Fig1. (a)), and according to the place of the specular spot, which is the sun's reflection, the deviation from the receiver is obtained. Two bars are suggested to be used: horizontal and vertical (Fig. 1(b)). Stainless-steel bars were used with 60 %–70 % reflectivity in the visible light; hence, it has both specular and diffuse reflection. While our focus is to develop a method for stopping the effect of shading and blocking totally, two bars may be placed on both left and right edges, so the total is three. The top part of the bar will not be shaded (especially in multi-tower systems), and the shading or blocking will be either on the right or left edge. As a result, we offer a method that is robust and not affected by shading or blocking.

The size of the spot is affected by the distance between the camera and the bar, and by the bar's curvature. In this experiment, the distance between the bar and the observer D is 100 m, the radius of curvature R is 20 m, and the spot L is 8.2 cm, according to the below calculation and considering only specular reflection (see Fig. 2).

ω - 0.009= -Φ

2Θ - 0.009= -Φ

2L/R - 0.009 = - L/D

However, the value of L increases because of diffusive reflection. A one-meter steel rod with high specular reflection is used (Fig. 3(a)), and the spread-out Gaussian pixel grey level distribution that represents the intensity of light along the bar B is shown in Fig. 3(b). All of the captured images were first converted to grayscale, where each pixel value represents the intensity or power [mW] of light that was captured at that specific location.

To define the curvature, we induced an optical sag at the center of the bar and held it at the two ends. According to the sag equation near zero, the radius of curvature can be calculated (Dereniak and Dereniak, 2008):

$$sag = \frac{L^2}{8R}$$

where L is the length of the bar and R is the radius of curvature. The sag

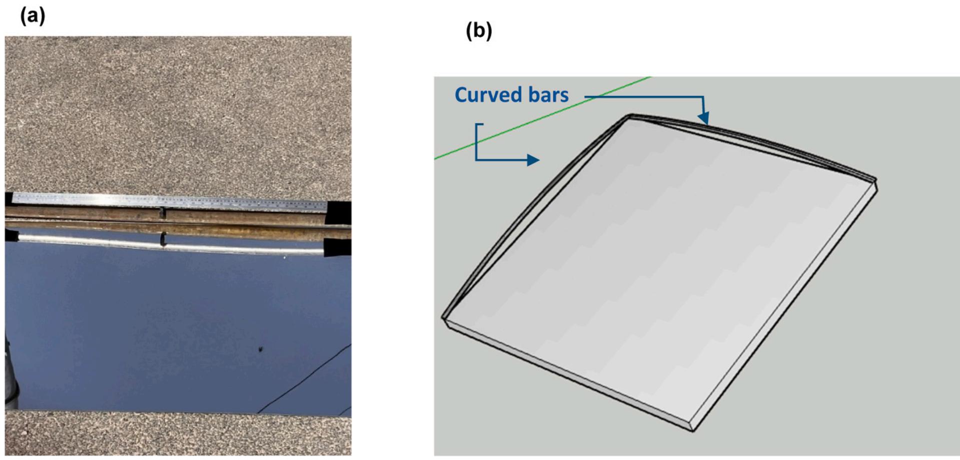

Fig. 1. (a) A mirror with an attached curved specular bar along its edge (b) Two horizontal and vertical bars attached to the heliostat.

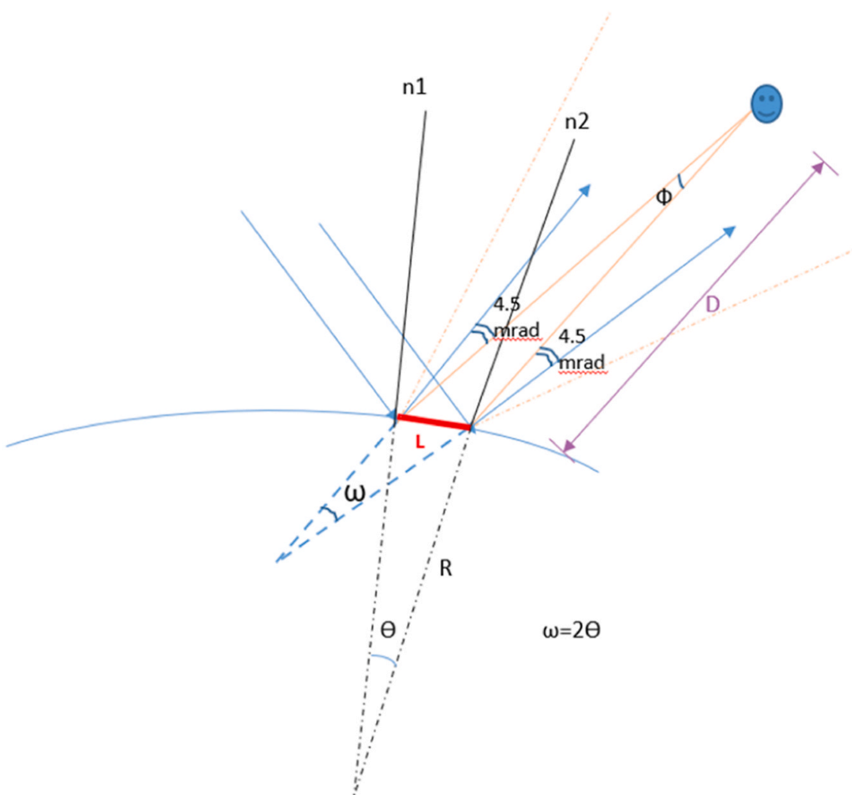

Fig. 2. Location and size of the spot on the bar as seen by a viewer.

is made at a base rigid rod with a length of 2 m, and a 1-meter steel bar is attached to it to ensure working in the paraxial approximation limit (Dereniak and Dereniak, 2008). We used a sag = 2.5 cm, then R= 20 m in the experiment.

Pictures were captured every 30.25 seconds, which means every 2.2 mrad movement of the sun. Neutral density filters with optical density = 4 were added to the CCD cameras. Optical density filters OD describe the logarithm (base 10) of the transmission, (OD1 =10 %, and OD2 =1 %) (Edmund-Optics, 2024). So, the brightness of the pictures decreases to 0.01 % of the original value. Filters are used in this process to adjust the amount of light that reaches the camera sensor within its dynamic range. The use of such filters helps in achieving more accurate representations of light intensity across a scene without saturation, thus ensuring that pixel values stay within the usable range (0−255). However, it's important to note that while these filters modify the intensity of light captured, they don't change the relationship between pixel values and the actual physical light intensity—rather, they scale the light intensity being recorded. The exposure time is manually set to 250 ms. The shift in the spot location is measured and related to the real shift in the sun location. First, the spot is extracted using Otsu's thresholding method (OTSU, 1979), a popular method for automatic image thresholding used to separate objects or regions of interest from the background in a grayscale image. The goal of thresholding is to find a threshold value that effectively divides the pixels into two classes: foreground and background. Otsu's method determines the optimal threshold value by the discriminant criterion, namely, to maximize the separability of the resultant classes in gray levels (OTSU, 1979), which means to maximize the variance between the two classes that the

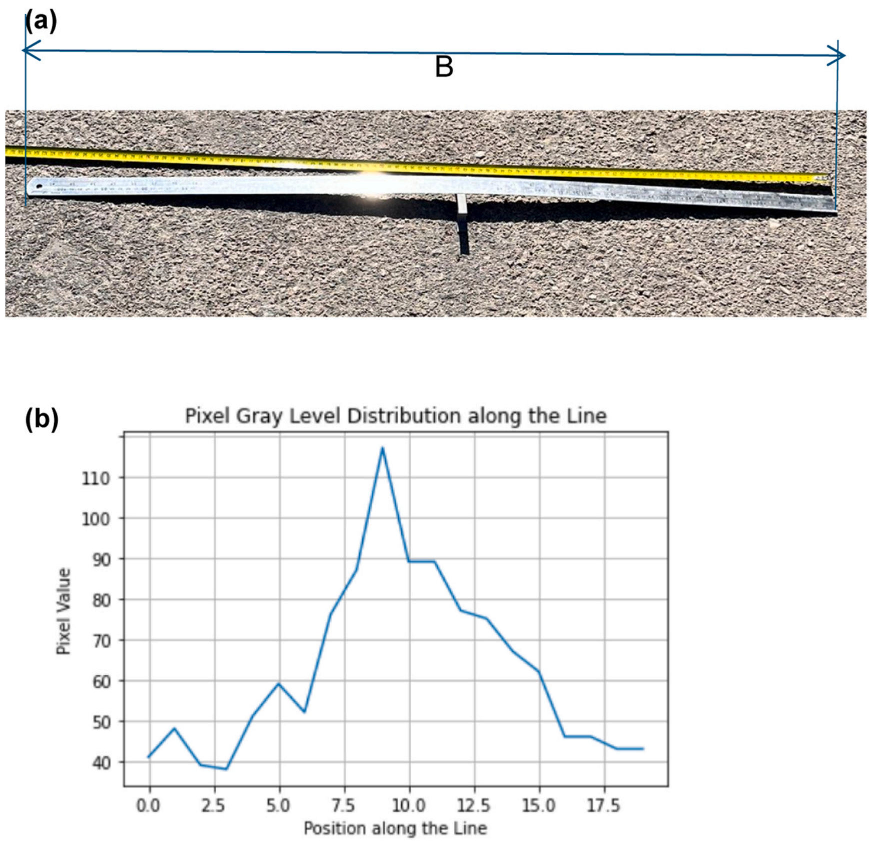

Fig. 3. (a) 1-meter steel bar used in the triangulation experiment (b) Spread-out Gaussian pixel grey level distribution along the steel bar.

foreground and background represent, which the formula can give (OTSU, 1979):

$\sigma^2_{\text{between}} = w1 \cdot w2 \cdot (\mu 1 - \mu 2)^2$

Where $w1$ and $w2$ are the probabilities of the two classes separated by the threshold, and $\mu 1$ and $\mu 2$ are the means of the two classes.

Second, the sub-pixel center of mass is calculated by obtaining the pixel-level center of mass using binary geometrical calculations (Zeghoudi, 2023), and then calculating the offsets from the center of mass using a *window weighted centroid method* (Zhou et al., 2016). It is based on the assumption that minor deviations from boundary pixels can be accumulated to give the major offset estimate of the grey-level center of mass. Assuming that the pixel-level centroid is calculated in the point ($X_{\circ}$, $Y_{\circ}$), the subpixel offsets from the pixel-level centroid s and t in the x and y positions, respectively, can be calculated by the equations:

$$s = \frac{\sum_{i=1}^{\text{contour area}} \sum_{j=1}^{\text{contour area}} (j - X_{\circ}) f(i,j)}{\sum_{i=1}^{\text{contour area}} \sum_{j=1}^{\text{contour area}} f(i,j)}$$

And

$$t = \frac{\sum_{i=1}^{\text{contour area}} \sum_{j=1}^{\text{contour area}} (i - Y_{\circ}) f(i,j)}{\sum_{i=1}^{\text{contour area}} \sum_{j=1}^{\text{contour area}} f(i,j)}$$

Where $f(i,j)$ is the pixel grey level value of the neighboring pixel, $(j - X_{\circ})$, $(i - Y_{\circ})$ are the shifts of that pixel from the center of mass in both the x and y directions.

Further enhancements could involve attaching specular spheres to these bars for absolute spot location determination without pre-calibration, as can be seen in Fig. 4 where two imaginary specular spheres were added to the two ends of the bar. Moreover, even with the shading of a part of the bar that causes one of the spheres to disappear, the position of the spot can still be detected by the distance to the other sphere.

We note that only shading and blocking of the sun's reflection from the bar may affect the triangulation method, however, the spot location and upper specular sphere are sufficient to calculate the heliostat position and is always at the upper half of the heliostat, which is unaffected at a reasonable GCR. Partial reflection due to blocking and shading, can be detected by image processing means, to optimize directing the partial reflection into the receiver's center. As far as we know, the ability to direct the partial reflection into the center of the receiver is unique to our method.

2.2. Prior art: captured intensity difference experiment

In Kribus' method, four cameras are installed around the receiver and directed towards the solar field to measure how much deviation each heliostat has from the focus target by comparing the power differences from each heliostat (Kribus et al., 2004). The cameras are placed around the focus target at a safe distance so that no direct reflected radiation would reach the cameras' sensors (see Fig. 5; Kribus

Fig. 4. Two (imaginary) specular spheres were added to the bar for absolute spot location determination without pre-calibration.

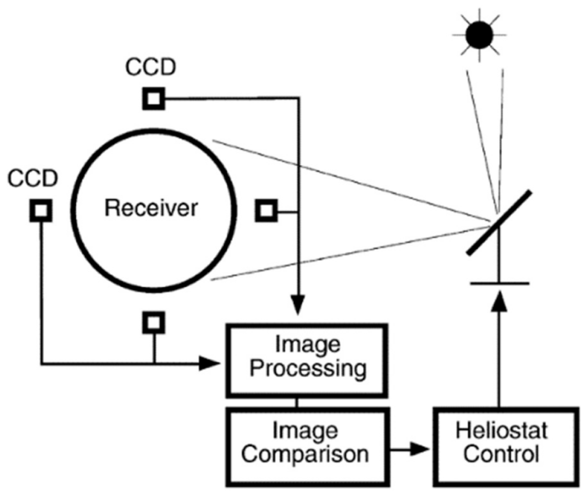

Fig. 5. Four cameras around the receiver in Kribus' method (Kribus et al., 2004).

et al., 2004). Then, the power difference between the two opposite cameras is measured and related to the offset from the target point (Kribus et al., 2004). Kribus presented a significant improvement in measurement accuracy (0.1–0.3 mrad) and a low-cost requirement compared to the total cost of heliostats. However, Kribus' method is tested on a single heliostat, so it didn't consider the shading and blocking effects. The reported value of the shading and blocking factor ranges from 20 % for the un-optimized case to 4 % for the optimized case at a solar elevation angle of 23.76° in a latitude of 26° N (Christoph Sattler et al., 2020), and can be even more. These values change the detected power in each camera, directly leading to significant errors in Kribus' method. Our experiment setup is shown in Fig. 6: A 10 mm* 10 mm silver mirror PF05–03-P01 (Anon, 2003) with reflectance > 97.5 % for 450 nm-2 µm is surrounded with Black Flocked self-adhesive paper with low reflectance < 3 % in the visible light (Anon, 2003) and attached to a Compact Stepper Motor Actuator with 25 mm travel, which in turn is controlled by K-Cube Stepper Motor Controller. The mirror is aligned opposite to a flashlight and a receiver, making an angle of 28° between the sun vector and the vector to the target. The flashlight is powered by a power supply of 4.5 volts and 0.1 amperes and has wavelengths similar to the solar light and 9 milliradians angle. The receiver has four USB 8MP Wide Angle Camera Modules (ArduCam) distanced 5 cm from each other. A laser and a SpotOn Analog Beam Positioner were used to measure the exact orientation of the mirror (Anon, 2025).

2.2.1. Calculate intensity difference

When each of the four cameras captures an image of the solar field, an algorithm finds the heliostat area by splitting it from the background using thresholding. Then, the intensity reeach camera from the heliostat is calculated by the function cv2.mean from the OpenCV library (Anon, 2024a; Cantoni et al., 2011), which calculates the value of each pixel, sums them up, and then divides them by the number of pixels. Finally, this value is normalized (divided by a reference value, a part of the picture that is supposed to have the same intensity in all four cameras) to eliminate the effect of exposure time differences between the cameras. The intensity difference between each two opposite cameras is inputted into the PID controller, and then the PID gives a manipulating value to the motor to move. This process continued for 13 s, then the controller stopped, and the final position of the mirror is recorded. See Fig. 7.

2.2.2. Shading and blocking effects

The same experiment is repeated but with putting another heliostat in the field that blocks the original one by 24 % (Fig. 8), to see how much that affects the accuracy of tracking.

3. Results

3.1. Curved specular bar experiment (triangulation)

The system's capability to detect deviation is tested by considering the sun's azimuth angle change with time. A picture is captured every

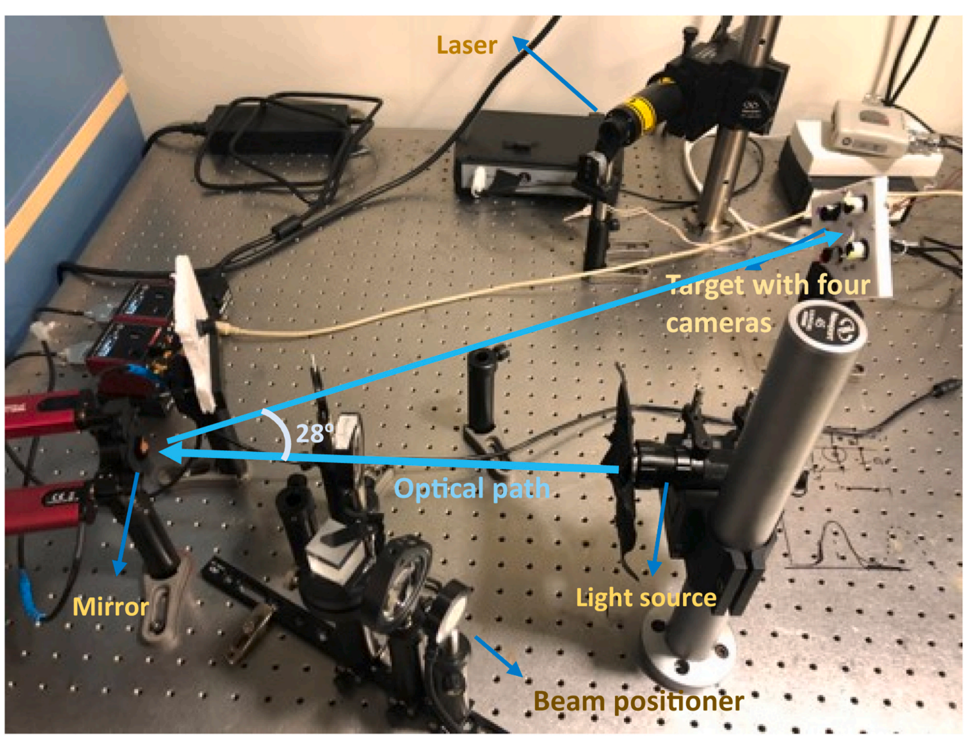

Fig. 6. Captured intensity difference experiment setup.

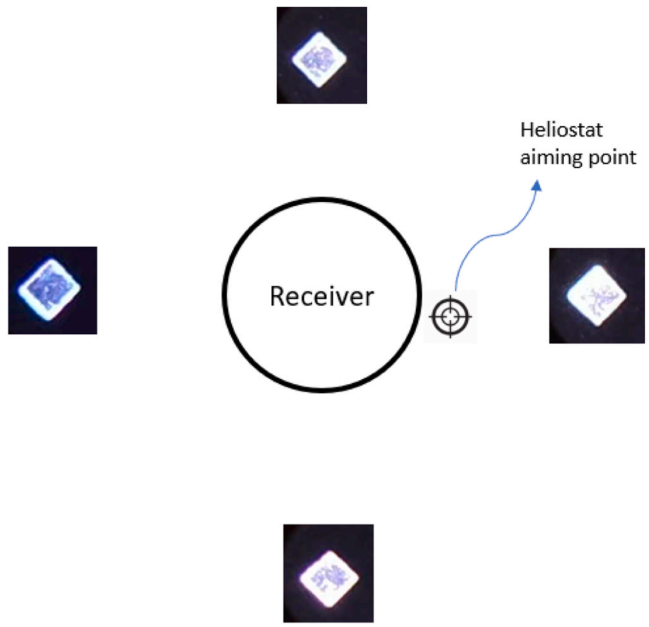

Fig. 7. Four pictures are captured from each cam, then the heliostat area is split from the background, and then the power reaching each camera from the heliostat is represented by the mean pixel value. Then, the difference in captured intensity between each two opposite cameras is calculated and related to the heliostat aiming point.

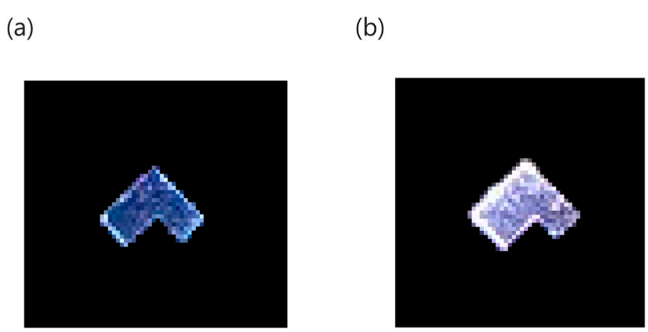

Fig. 8. Image of the heliostat after splitting it from the background captured by a) left camera and b) right camera.

30.25 seconds, which is 2.2 mrad of the sun's movement. The bar is oriented east-west and angled 40 degrees with the ground.

By calculating the sub-pixel center of mass of the appeared spot, the coefficient of determination (R2) for the regression line between the real deviation in mrad and the pixels shift on the bar as shown from a 100-meter distance by an 8.3-megapixel camera is 0.9978 (Fig. 9). The error detection accuracy is at an RMSE accuracy of 0.8 mrad.

3.2. Prior art: captured intensity difference experiment

As a reference, we start with a non-shaded heliostat and demonstrate its tracking accuracy. Next, we induce shading into the setup and show how it affects the tracking accuracy.

3.2.1. Captured intensity difference experiment without shading or blocking

First, many pictures were captured using the four cameras and the heliostat area is cut by threshold to obtain the average brightness value of the heliostat from each of the four pictures. After that, the relative intensity difference between the pictures from each two opposite cameras is calculated and related to the actual deviation measured by the beam positioner. The relation between the deviation from the focus

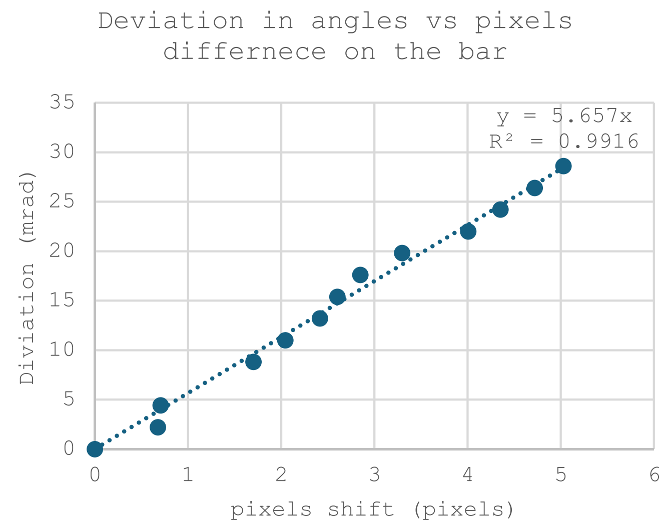

Fig. 9. Relation between Deviation (mrad) and the shift in the center of the spot on the bar (pixels).

target and the intensity difference between the two opposite cameras is monotonic, shown in Fig. 10. The root mean squared error value (RMSE) was calculated by taking the average of the squared error of estimated deviation and real deviation. Estimated deviation was calculated by relating the brightness differences to the deviation value. The root mean squared error value is 0.8 milliradians.

3.2.2. Captured intensity difference experiment with 24 % blocking

With 24 % blocking of the heliostat, it is shown in Fig. 11 (a) the relation between the deviation from the focus target in milliradians and the brightness difference. The relation is still monotonic and has a high correlation coefficient (R^2). However, a further shift of 4 milliradians can be seen in the controller's accuracy (the amount of shift between mirror's final orientation and correct orientation) when returning to the focus target after different initial manual offset (Fig. 11 (b)). This shift caused by shading cannot be overcome because it is an unpredictable error that changes according to the surrounding conditions. The error happens even though we are concerned with the average grey value of the pixels and not with something related to the count of pixels. The reason for that is that the intensity profile across the heliostat is not uniform and unpredictable. The controller's accuracy in returning to the desired position is around four milliradians.

4. Conclusion

This study investigated the heliostat control method for achieving continuous, accurate tracking in heliostat field systems without interfering with the receiver's operation. Our method involves triangulation using curved specular bars placed along heliostat edges having specular spheres at its edges, to determine deviations from the receiver without disrupting heliostat operation. This method showcased better accuracy compared to prior art at 0.8 mrad, considering shading and blocking scenarios. It also gives the best exploitation of pixels. As far as we know this is the only method that optimizes the partial reflection of heliostat into the receiver's center.

This method offers promising applications for large-scale CSP and modular multi-tower systems with grid parity, paving the way for efficient and accurate heliostat tracking in solar energy harvesting.

CRediT authorship contribution statement

Abunajeeb Irjuwan: Writing – original draft, Investigation, Data curation. **Stein Gideon:** Conceptualization. **Rotschild Carmel:** Writing

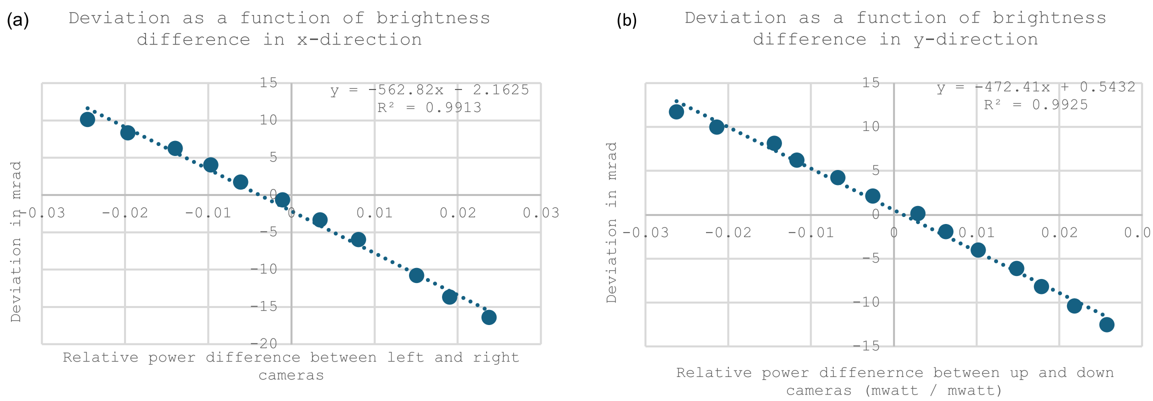

Fig. 10. Relation between the deviation from the focus target in milliradians and the brightness difference in (a) x-direction and (b) y-direction.

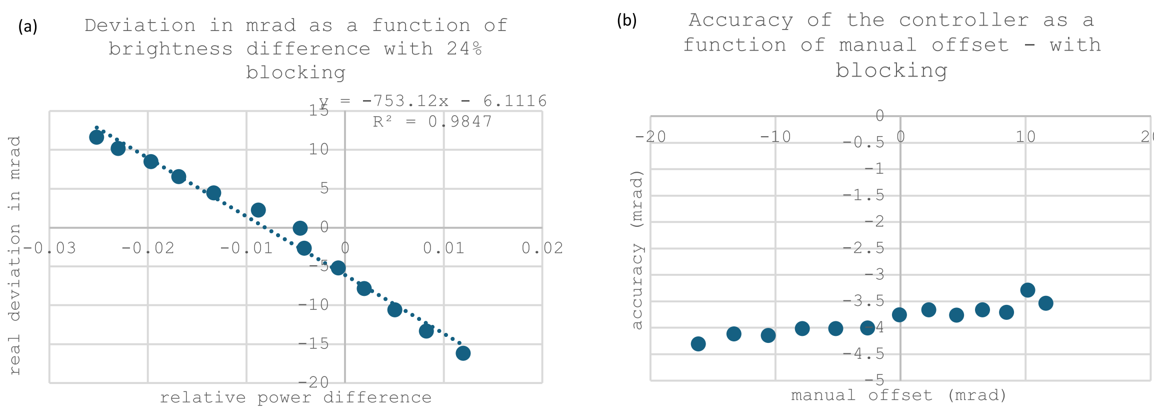

Fig. 11. Experiment results when the heliostat is 24 % blocked: (a) Relation between the real deviation from the focus target in milliradians and the intensity difference. (b) Accuracy of the controller when returning to the focus target after different initial manual offset values.

– original draft, Supervision, Resources, Funding acquisition, Conceptualization.

Declaration of Competing Interest

The authors declare that they have no known competing financial interests or personal relationships that could have appeared to influence the work reported in this paper.

Acknowledgement

The research leading to these results was supported by The Nancy and Stephen Grand Technion Energy Program, The Leonard and Diane Sherman Interdisciplinary Graduate School Fellowship, SolarEdge Technologies Ltd., as part of the Guy Sela Memorial Project at the Technion.

Data availability

Data will be made available on request.

References

Anon, "Thorlabs:Products," Thorlabs, 2003. [Online]. Available: ⟨https://www.thorlabs.com⟩.
Anon, "Heliogen," 07 December 2023. [Online]. Available: ⟨https://www.heliogen.com/press-releases/heliogen-unveils-significant-achievement-in-concentrating-solar-technology-with-successful-demonstration-of-advanced-control-software-at-sandia-labs/?utm_source=chatgpt.com⟩. [Accessed 05 March 2025].
Anon "OpenCV Documentation," OpenCV organization, [Online]. Available: ⟨https://docs.opencv.org/4.x/dc/dbb/tutorial_py_calibration.html⟩. [Accessed 20 3 2024a].
Anon, (2025) "Duma Optronics: Projects: Position Sensing: SpotOn Analog," Duma Optronics LTD, [Online]. Available: ⟨https://www.dumaoptronics.com/spoton-analog⟩.
Bern, G., Schöttl, P., Heimsath, A., Nitz, P., 2017. Novel imaging closed-loop control strategy for heliostats. AIP Conf. Proc.
Cantoni, V., Levialdi, S., Zavidovique, B., 2011. 2 - Visual Cues. 3C Vision. Elsevier, pp. 19–113.
Christoph Sattler, J., Röger, M., Schwarzbözl, P., Buck, R., Macke, A., Raeder, C., Göttsche, J., 2020. "Review of heliostat calibration and tracking control methods. Sol. Energy 207, 110–132.
Coquand, M., Caliot, C., Hénault, F., 2017. Backward-gazing method for heliostats shape errors measurement and calibration. AIP Conf. Proc.
Dereniak, E.L., Dereniak, T.D., 2008. Curved optical surfaces. Geometrical and Trigonometric Optics. Cambridge University Press, pp. 96–121.
Díaz-Félix, L., Escobar-Toledo, M., Waissman, J., Pitalúa-Díaz, N., Arancibia-Bulnes, C., 2014. Evaluation of heliostat field global tracking error distributions by Monte Carlo simulations. Energy Procedia 49, 1308–1317.
Edmund-Optics, "Understanding Neutral Density Filters," Edmund Optics, 2024. [Online]. Available: ⟨https://www.edmundoptics.com/knowledge-center/application-notes/optics/understanding-neutral-density-filters/⟩. [Accessed 2024].
El Ydrissi, M., Ghennioui, H., Bennouna, E.G., Farid, A., 2019. A review of optical errors and available applications of deflectometry technique in solar thermal power applications. Renew. Sustain. Energy Rev. 116, 1364-0321.
Google, (2025) "Heliostat Control and Targeting," google.org.
He, Y.-L., Cui, F.-Q., Cheng, Z.-D., Li, Z.-Y., Tao, W.-Q., 2013. Numerical simulation of solar radiation transmission process for the solar tower power plant: from the heliostat field to the pressurized volumetric receiver. Appl. Therm. Eng. 61 (2), 583–595.
B.E. Hines and R.L. Johnson.US Patent W O 2012/125751 A2, 2012.
Hu, T., Deng, Z., Tian, J., Wang, Y., 2021. A comprehensive mathematical approach and optimization principle for solar flux distribution and optical efficiency in a solar tower. Appl. Therm. Eng. 182.
Klimek, J., Sauerborn, M., Hoffschmidt, B., 2012. Radar technology for heliostat position control. Sol. Paces Conf. Marrakesh.
Kribus, A., Vishnevetsky, I., Yogev, A., Rubinov, T., 2004. Closed loop control of heliostats. Energy 29, 905–913.
Krupkin, A., Yogev, V., 1999. Control of a heliostat field in a solar energy plant. United States Patent US5862799A, 26 01.

Md Tasbirul, I., Nazmul, H., A. A.B, S. R, 2018. A comprehensive review of state-of-the-art concentrating solar power (CSP) technologies: Current status and research trends. Renew. Sustain. Energy Rev. 91, 987–1018.

OTSU, N., 1979. A threshold selection method from gray-level histograms. EEE Trans. Systrems Man Cybern. SMC-9 (1), 62–66.

Palacios, A., Barreneche, C., Navarro, M., Ding, Y., 2020. Thermal energy storage technologies for concentrated solar power – a review from a materials perspective. Renew. Energy 156, 1244–1265.

Reddy, D., Khan, M., 2022. Stationary point focus solar concentrators—a review. Int. J. Energy Res.

del Ríoa, P., Peñasco, C., Mir-Artigues, P., 2018. An overview of drivers and barriers to concentrated solar power in the European Union. Renew. Sustain. Energy Rev. 81, 1019–1029.

Rizvi, A.A., Yang, D., 2022. A detailed account of calculation of shading and blocking factor of a heliostat field. Renew. Energy 181, 292–303.

Sánchez-González, A., Grange, B., Caliot, C., 2020. Computation of canting errors in heliostats by flux map fitting: experimental assessment. Opt. Express 28 (26), 39868–39889.

Sioshansi, R., Denholm, P., 2010. The value of concentrating solar power and thermal energy storage. IEEE Trans. Sustain. Energy 1, 173–183.

Zavodny, M., Slack, M., Huibregtse, R., Sonn, A., 2015. Tower-based CSP artificial light calibration system. Energy Procedia 69, 1488–1497.

Zeghoudi, A., 2023. Solar power heliostat control using image processing technology and artificial neural networks. J. Eur. Des. Syst. Autom. Edmont. 56 (1), 165–171.

Zhou, F., Zhao, J., Ye, T., 2016. Fast star centroid extraction algorithm with sub-pixel accuracy based on FPGA. Real. Time Image Proc. 12, 613–622.